Unexpected 13N concentrations in ISIS synchrotron room air

B Jones, G J Burns, H V Cavanagh, D J S Findlay, S Karbassi, N A Nilsson, 3 G P Škoro and P N M Wright

Published version information

Citation: B Jones et al. 'Unexpected 13N concentrations in ISIS synchrotron room air.' Appl Radiat Isotopes 182 (2022): 110139.

DOI: 10.1016/j.apradiso.2022.110139

Unexpected ^{13}N concentrations in ISIS synchrotron room air

B Jones, G J Burns, H V Cavanagh, D J S Findlay*, S Karbassi, N A Nilsson, G P Škoro and P N M Wright

ISIS, Rutherford Appleton Laboratory, Chilton, Oxfordshire, UK

(* Corresponding author: david.findlay@stfc.ac.uk)

Abstract

The specific activity of air in the large open room housing the 800-MeV proton synchrotron of the ISIS Spallation Neutron and Muon Source has been measured. Air from several positions within the ISIS synchrotron room was sucked through a long flexible tube, and run past a shielded HPGe gamma-ray detector outside the synchrotron room. In spite of an expectation that ^{13}N should be the largest component of the overall activity in the air, the results of the measurements are consistent with the presence in the air of ^{11}C and ^{41}Ar only, and suggest that the activity in the air is mostly created not in the synchrotron room itself but in the massive shielding monoliths around the neutron-producing targets, monoliths through which ventilation air is drawn into the synchrotron room. Typical specific activities of ^{11}C and ^{41}Ar in the air in the synchrotron room are ~0.10 and ~0.03 Bq cm^{-3} respectively, the upper limit for ^{13}N being at most ~0.01 Bq cm^{-3}.

1. Introduction

The ISIS Spallation Neutron and Muon Source [1, 2] is driven by an 800-MeV ~250-μA proton synchrotron running at 50 pulses per second (pps), the synchrotron in turn being driven by a 70-MeV H^- drift tube linac. The proton beam from the synchrotron is split and delivered at 40 pps to Target Station 1 (TS-1) and at 10 pps to Target Station 2 (TS-2). Accelerator, proton beam line and target areas are ventilated to avoid build-up of toxic and corrosive gaseous products, to remove heat, to maintain machine areas slightly below atmospheric pressure, and to facilitate the entry of personnel into machine areas after the beam has been switched off.

At ISIS, the synchrotron is located in an open room 61 metres in diameter and 9 metres in mean height, and this large room acts as a ~3-hour delay/decay tank. Air is drawn into the ~25000-m^3 synchrotron room from ventilated areas around the neutron-producing targets and the proton beam lines through the two ~100-metres-long tunnels for the extracted proton beam lines, and air is extracted from the synchrotron room at a rate of 2 m^3 s^{-1} and discharged to atmosphere (authorised by the UK Environment Agency). A schematic diagram is shown as Fig. 1.

Whilst previous calculations [3] (discussed in Sect. 4 below) of specific activities of air in the ISIS synchrotron room indicated that ^{13}N was likely to be the largest component of the overall activity, measurements made over several years using equipment for monitoring gaseous discharges have suggested that there is significantly more ^{11}C activity than ^{13}N activity in the air [4]. The work reported in this paper was carried out both to measure directly the specific activity of the air in the synchrotron room and to try to resolve the question of the relative contributions of ^{11}C and ^{13}N activity. This paper deals only with contributions to activity in the air from ^{11}C, ^{13}N, ^{15}O and ^{41}Ar.

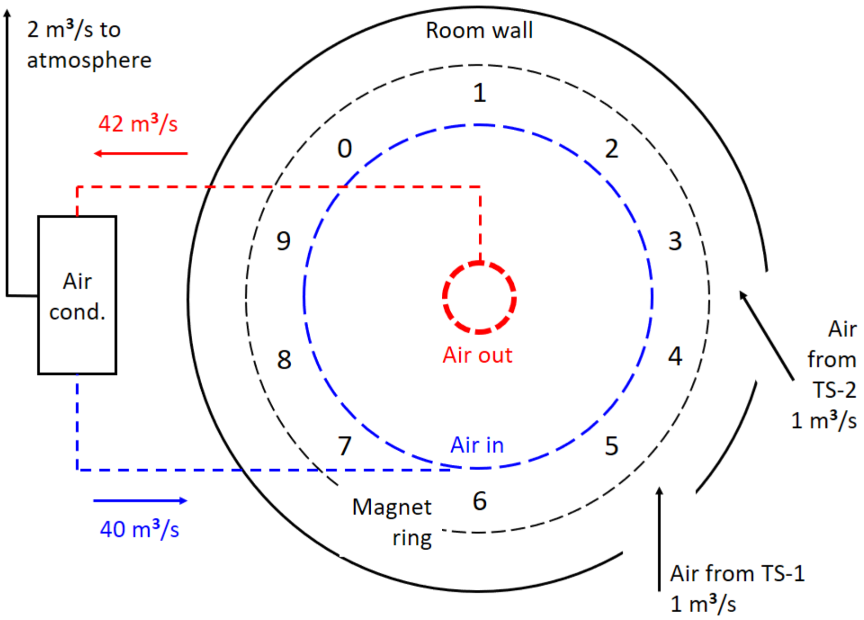

Fig. 1. Schematic diagram of air flows into and out of the ISIS synchrotron room. Air from the full-flow-filtered air-conditioning system enters at floor level, and leaves at ceiling level. The numbers 0–9 denote the positions of the ten superperiods (SPs) of the synchrotron (injection takes place in SP0, and collimation and extraction take place in SP1). The air from Target Stations TS-1 and TS-2 is essentially ventilation air from the shutter voids in the several-thousands-of-tons monoliths of steel and concrete shielding around the neutron-producing targets. In order to be able to switch on and off beams of neutrons to the research instruments in the experimental halls independently, massive ~20-ton movable steel shutters are incorporated in the monoliths, and the shutter voids are the voids in the steel monoliths necessary to accommodate the movement of the shutters. Air is discharged to atmosphere at a nominal rate of 2 $m^3 s^{-1}$ through a stack on the roof of the air-conditioning building.

2. Measurements

Since the synchrotron and its surroundings become radioactive in use, it is not practical to make measurements of activated air within the synchrotron room simply by using a health physics monitor, since background from activated machine components and support structures is always present. Consequently, a method was developed whereby air from the synchrotron room is sucked out along a 76-metre length of 10-cm-diameter flexible PVC air ducting hose, a fraction of this air is then circulated through a thin-walled aluminium cylindrical vessel with an internal volume and diameter of 859 cm^3 and 9.3 cm respectively immediately in front of a shielded Canberra BE3825 HPGe gamma-ray detector, and the air is then returned to the synchrotron room. The time for activated air to travel from the input end of the long flexible tube to the HPGe was measured using a smoke generator and found to be 69 ± 5 seconds [5]. A schematic diagram is shown in Fig. 2.

Successive 15-minute-long gamma-ray spectra[1] were recorded and stored over periods of two or three days — each period usually beginning just before the end of an irradiation campaign ('user cycle') and ending after a further ~1–2 days of accelerator physics work. A typical gamma-ray spectrum when the synchrotron was running steadily is shown in Fig. 3, in which the only gamma-ray lines of immediate significance are at 511 keV (from positron emitters such as ^{11}C, ^{13}N and ^{15}O) and at 1294 keV (from ^{41}Ar from neutron capture on the ~1% of argon naturally present in air). The beginnings and ends of counting periods were taken from the corresponding times recorded within the spectrum files themselves (correcting for two changes of local time from GMT (Greenwich Mean Time) to BST (British Summer Time)). Fig. 4 shows a representative set of data collected: counts per 15 minutes in 511- and 1294-keV peaks, and beam current from the synchrotron measured at 4-minute intervals.

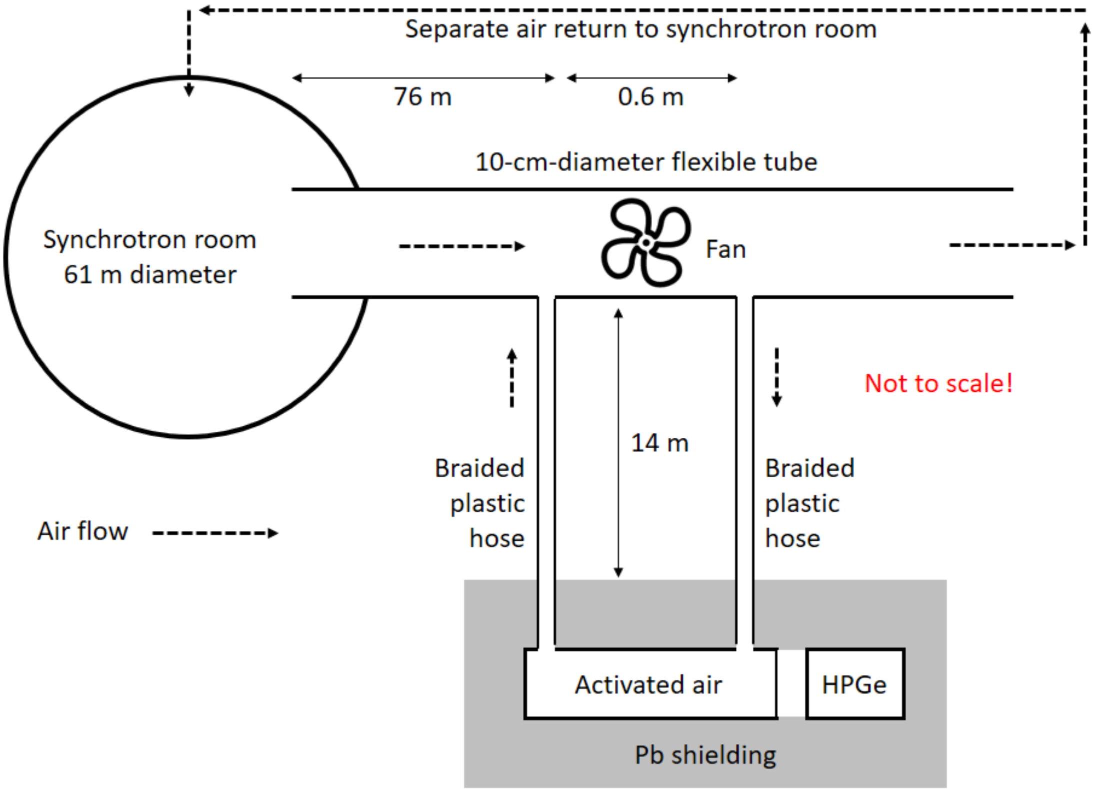

Fig. 2. Schematic representation of air from the ISIS synchrotron room being passed in front of the HPGe gamma-ray detector. Not to scale! The internal diameter and length of the activated air sample vessel in front of the HPGe detector were 9.3 and 12.7 cm respectively. The distance between the end of the activated air cylinder and the HPGe crystal was 1.0 ± 0.5 cm. The activated air is moved through the activated air sample vessel in front of the HPGe detector by the pressure difference across the fan.

[1] The spectra for the December 2019 and February 2020 sets of data were each 30 minutes long, not 15 minutes long.

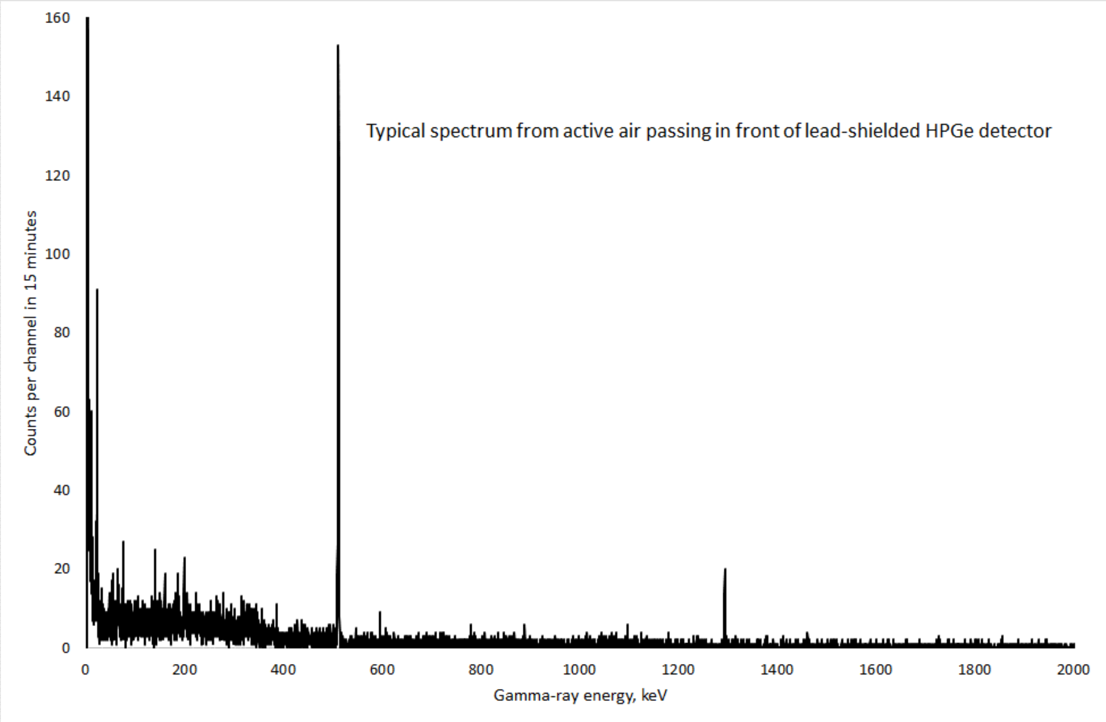

Fig. 3. Typical gamma-ray energy spectrum seen by the HPGe detector. The lines at 511 keV from positron-emitting radionuclides such as ^{11}C, ^{13}N and ^{15}O, and at 1294 keV from ^{41}Ar stand out very clearly.

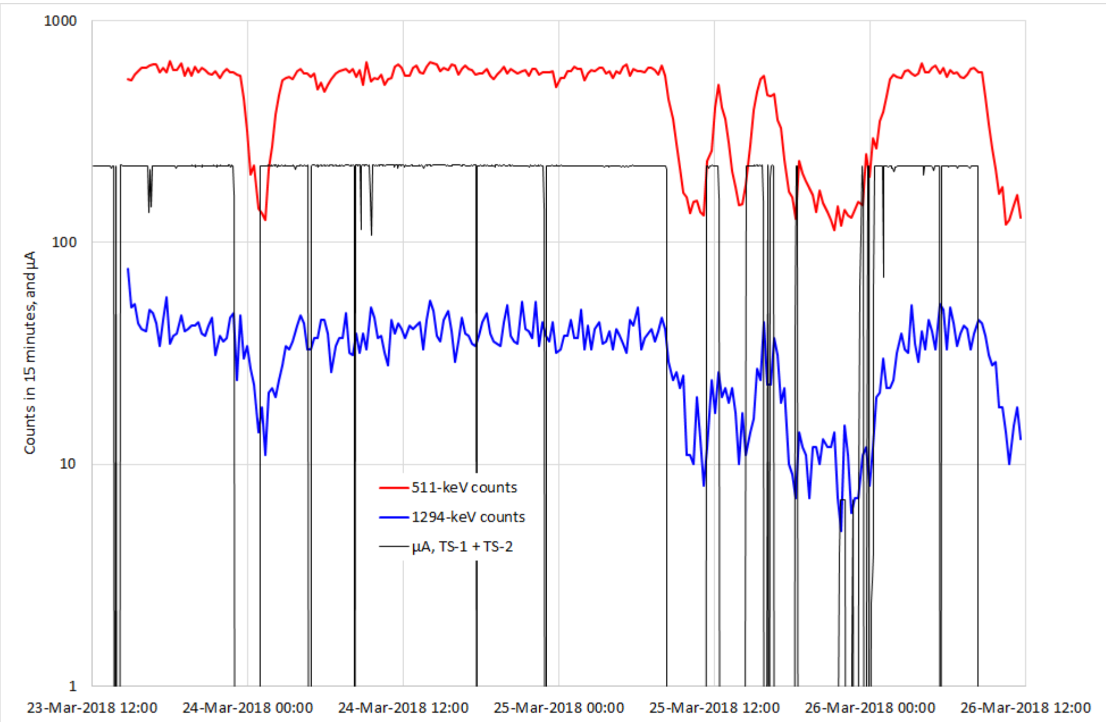

Fig. 4. Representative data set covering three days: counts in 15 minutes in 511- and 1294-keV peaks in gamma-ray spectra, and the synchrotron proton beam current (which is also the sum of beam currents delivered to target stations TS-1 and TS-2).

3. Analyses

3.1 Model

In order to extract information from sets of data such as the set illustrated in Fig. 4, the following model was adopted. Assume atoms of radionuclides i are produced by the proton beam at rates $r_i\, I$ where I is the proton beam current and r_i is a constant of proportionality (atoms μA^{-1} s^{-1}). Suppose activated air takes time δ_s to get from wherever it is produced to the synchrotron room. Then in time dt the number of atoms of radionuclide i appearing at time t in the synchrotron room is

$$dN_i = \exp(-\lambda_i \delta_s)\, r_i\, I(t-\delta_s)\, dt$$

where $\lambda_i = \ln(2)/t_{1/2,i}$ is the decay constant for radionuclide i and $t_{1/2,i}$ is its half-life. Suppose there are N_i atoms of radionuclide i in the synchrotron room at time t, and suppose the air exchange rate and synchrotron room volume are v (m^3 s^{-1}) and V (m^3) respectively. Then, in time dt, $\lambda_i\, N_i\, dt$ atoms decay, and $(v/V)\, N_i\, dt$ atoms are removed. So the net change in number of atoms of radionuclide i in the synchrotron room is $dN_i = \exp(-\lambda_i \delta_s)\, r_i\, I(t-\delta_s)\, dt - \lambda_i\, N_i\, dt - (v/V)\, N_i\, dt$, which may be re-written as

$$dN_i = \exp(-\lambda_i \delta_s)\, r_i\, I(t-\delta_s)\, dt - \lambda_i'\, N_i\, dt$$

where $\lambda_i' = \lambda_i + v/V$. Since $I = I(t)$ is a known function of time ($I(t)$ is measured and recorded in 4-minute steps), $N_i = N_i(t)$ may be obtained by numerical integration, and thereby activities in the synchrotron room $\lambda_i N_i = \lambda_i N_i(t)$ may be obtained.

Suppose it takes time δ_c for the activated air to get from the synchrotron room to the HPGe detector, and assume that the gamma-ray emission probability for radionuclide i is α_i and that the HPGe detection efficiency for gamma-rays from radionuclide i is ε_i. Then the number of HPGe counts $c_{i,j}$ from radionuclide i over a counting interval Δ beginning at time t_j is

$$c_{i,j} = c_i(t_j + \Delta) = \alpha_i\, \varepsilon_i \int_{t_j}^{t_j+\Delta} \exp(-\lambda_i \delta_c)\, \lambda_i N_i(t-\delta_c)\, dt.$$

By fitting to the data by minimising the chi-squared per degree of freedom $\chi^2_{\mathrm{pdf}} = \{\sum_i (\sum_j (C_{i,j} - B_i - c_{i,j})^2/\delta C_{i,j}^2)\}/\{mn - (2m+2)\}$ where m is the number of radionuclides, parameters r_i, δ_s, δ_c and B_i may be extracted, where i runs from 1 up to m, the C_i's are the measured counts corresponding to radionuclide i, B_i is the corresponding background, and j runs from 1 up to n where n is the number of counting intervals.

If the passage of activated air from the source of production to the synchrotron room is characterised not by a unique time but by a symmetrical distribution of times spanning a finite range $2w$ described by a normalised function $s(\varepsilon) = s(\bar{t}, \varepsilon)$ where $\bar{t}$ is the mean time and ε is the deviation from the mean time (as will be seen to be the case in Sect. 3.3), the resultant number of atoms $N_i{}'(t)$ of radionuclide i may be obtained from $N_i{}'(t) = \int_{-w}^{w} N_i(t-\varepsilon)\, s(\varepsilon)\, d\varepsilon$.

3.2 Half-life of 511-keV component

It is clear that the half-life of the 1294-keV component should correspond to the 110-minute half-life of ^{41}Ar, but the 511-keV component could be due to some or all of ^{11}C, ^{13}N and ^{15}O with half-lives of 20.3, 9.96 and 2.03 minutes respectively, since these three radionuclides can all be produced by nuclear reactions in the air and they emit only positrons when they decay. Fig. 5 shows the 511-keV component for a typical beam-on-to-beam-off transition. Also shown is the rate at which ^{11}C alone would decay, taking into account the air extraction rate from the synchrotron room, *i.e.* the dashed line is proportional to $\exp(-\lambda'\,(t-t_0))$ where $\lambda' = \lambda_{11_C} + v/V$ is the effective ^{11}C decay constant, $\lambda_{11_C} = \ln(2)/t_{1/2,11_C}$ where $t_{1/2,11_C} = 20.3$ minutes, v and V are as set out in Sect. 3.1 above and have values of 2 m s^{-1} and 25000 m^3 respectively, and t_0 is the beam-off time. Since the effective half-life $t'_{1/2} = \ln(2)/\lambda' = 17.8$ minutes, it seems clear that the measured data support the conclusion that the 511-keV activity is mostly due to ^{11}C alone.

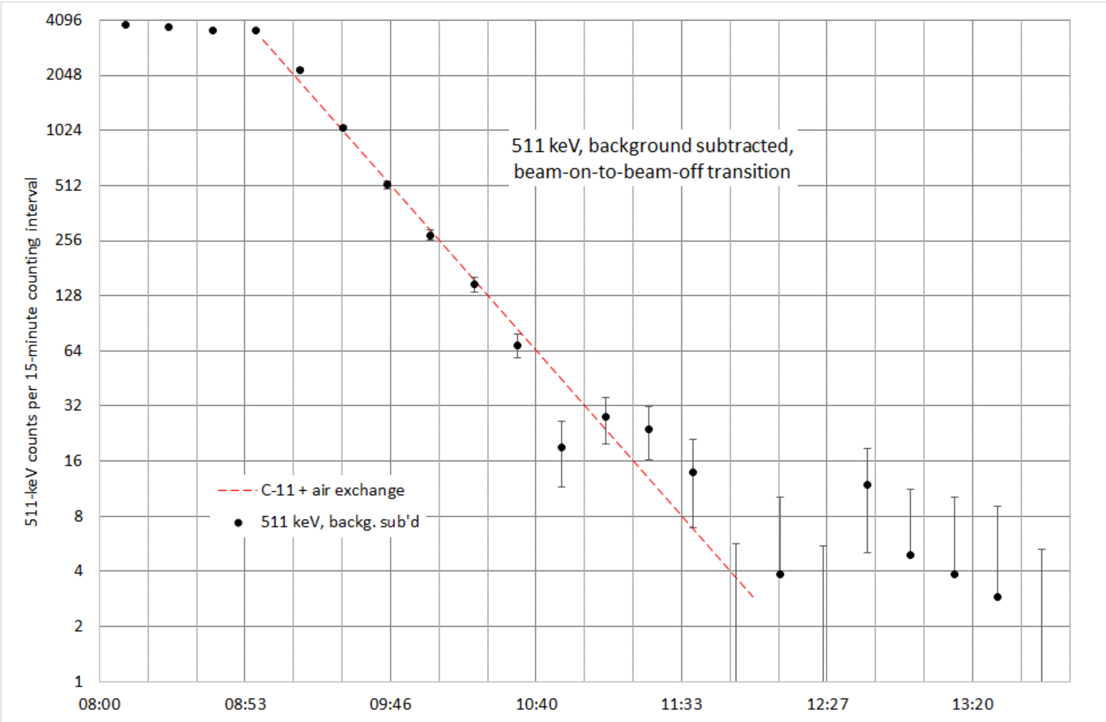

Fig. 5. 511-keV component of counts in HPGe detector after background subtraction for a typical beam-on-to-beam-off transition, plotted on a base-2 logarithmic scale with 17.8-minute intervals (the effective ^{11}C half-life taking into account air exchange in the synchrotron room) marked on the horizontal axis. The dashed line is a decay proportional to $2^{-t/(17.8\text{ minutes})}$. It is evident that the decay corresponds almost entirely to the decay of ^{11}C.

This conclusion, *viz* that the 511-keV activity is mostly due to ^{11}C alone, is at variance with the results of Monte Carlo calculations [3] of saturation specific activities of air in the synchrotron room using MCNPX and CINDER-90 [6, 7] that were referred to in Sect. 1. Whilst these preliminary calculations involved some significant assumptions and approximations, the results suggested that saturation activities of ^{11}C, ^{13}N, ^{15}O and ^{41}Ar in the synchrotron room air should be in ratios of roughly 8±5 : 72±5 : 2^{+5}_{-2} : 18±5. How can the difference between these calculated results and the results of the present measurement be best explained? Consideration of this question is deferred until Sect. 3.5 below.

3.3 Delay times

With the assumption that that the 511-keV component seen by the HPGe detector is due to ^{11}C alone (so that in Sect. 3.1 $m = 2$), eight data sets (the one shown in Fig. 4 and seven others) were fitted using the model set out in Sect. 3.1. A typical fit is shown in Fig. 6, and results are set out in Table 1. However, in view of the possibility that the 511-keV component does in fact contain a significant contribution from ^{13}N, Table 1 also lists results assuming that the 511-keV component seen by the HPGe detector is due to ^{13}N alone. Whilst some of the fits in Table 1 are undoubtedly poor, the explanation being that the fits include periods of time when the synchrotron was not running normally but was being used for accelerator physics purposes when beam delivery and beam conditions are often well outside normal operational envelopes, it is evident that the fits are on average better assuming that the 511-keV component is due to ^{11}C alone than assuming it to be due to ^{13}N alone, and that the overall time from source to detector ranges between roughly 12 and 20 minutes depending on location within the synchrotron room.

With what can these times be compared? At ISIS the most likely places for air to be activated are the shutter voids in the massive shielding monoliths surrounding the neutron-producing targets (see caption to Fig. 1) where high fluxes of neutrons pass through the ventilating air. Elsewhere, little activity in air is likely to be produced, as beam losses around the synchrotron and along the proton beam transport lines are low [8] — confirmation being that when beam losses around the synchrotron were deliberately doubled no increase in activation was observed. Using a smoke generator, the mean time for air to be moved by the ventilation systems from the shutter voids to the synchrotron room was measured [9] as 8 minutes, with a spread of ±4 minutes. This mean time of 8 minutes, with two additions, *viz* the few minutes for air to be moved by the air-conditioning system within the synchrotron room from the point where the air from the shutter voids enters the synchrotron room to the point where the air is sampled, and the ~1 minute for air to travel from the sampling point to the HPGe gamma-ray detector, is in satisfactory agreement with the ~12–20 minutes obtained from the fits.

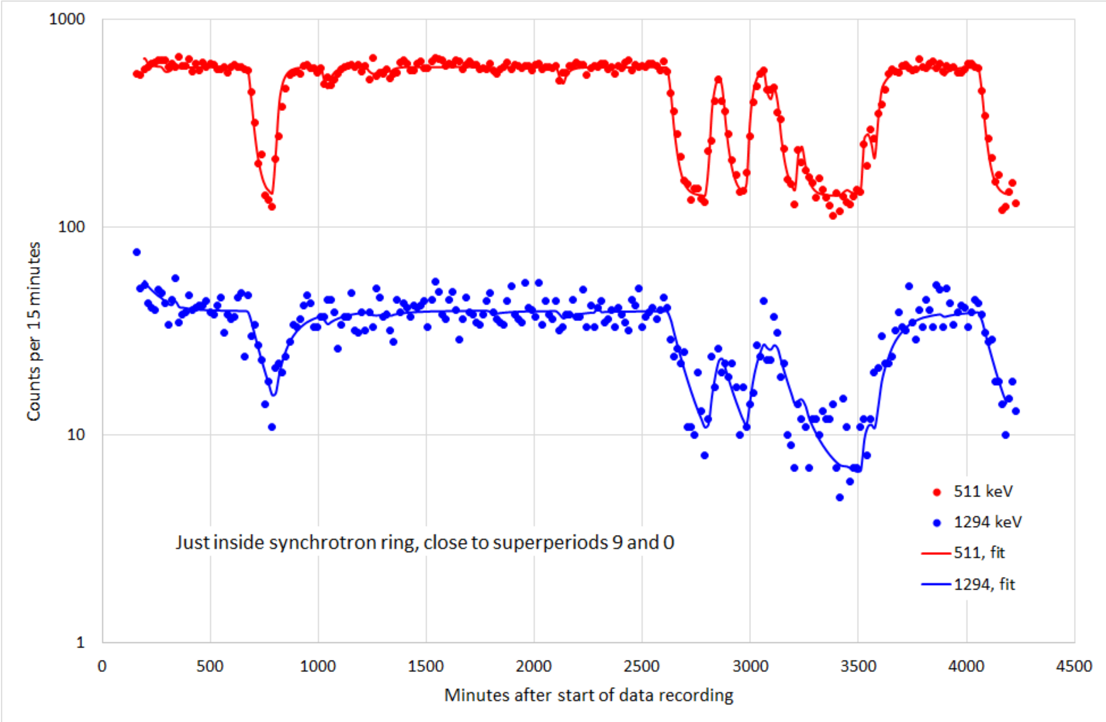

Fig. 6. Fits to 511- and 1294-keV data measured during 23–26 March 2018 according to the model described in Sect. 3.1. In this figure (Fig. 6) the data points are the $C_{i,j}$'s in Sect. 3.1, and the fitted lines are the $c_{i,j}$'s. Values of fitted parameters are listed in Table 1.

Date of measurement	Location from which air being sampled is drawn	511 keV = ^{11}C		511 keV = ^{13}N	
		$\delta_s + \delta_c$, minutes	χ^2_{pdf}	$\delta_s + \delta_c$, minutes	χ^2_{pdf}
Feb. 2018	Foil change area, SP0	15.1 ± 0.3	3.99	22.6 ± 8.01	6.48
Mar. 2018	SP0/9 datum points	18.2 ± 2.1	2.05	26.6 ± 12.4	3.46
May 2018	SP9 datum and SP6 bridge	16.8 ± 1.0	7.49	23.6 ± 1.5	11.4
Jul. 2018	Inner side of SP5/6	15.0 ± 0.6	19.2	15.2 ± 0.5	21.2
Oct. 2018	Inner side of SP5/6	14.0 ± 0.5	31.5	14.0 ± 0.9	21.8
Dec. 2018	Inner side of SP5/6	14.2 ± 0.4	20.1	14.8 ± 0.4	30.6
Apr. 2019	Inner side of SP5/6	15.0 ± 1.4	23.7	17.1 ± 2.3	34.2
Dec. 2019	Inner side of SP5/6	12.5 ± 0.7	87.3	14.8 ± 8.6	93.6
Feb. 2020	[Data timings unavailable]				

Table 1. Sums of source-to-synchrotron-room and synchrotron-room-to-HPGe delay times from fitting eight sets of data (the individual delay times δ_s and δ_c are essentially completely anti-correlated) for two 'extreme' assumptions, *viz* assuming that the 511-keV activity is due entirely to ^{11}C, and assuming that the 511-keV activity is due entirely to ^{13}N. The fits include incorporation of a rectangular distribution s as described in Sect. 3.1 spanning a range of ±4 minutes representing the spread in the nominal time δ_s for activated air to travel from the production source to the synchrotron room. The uncertainties quoted were obtained by perturbing one hundred times the counts $C_{i,j}$ per 15-minute counting period (see Sect. 3.1) by amounts chosen from random gaussian distributions with standard deviations $\delta C_{i,j}$ and then taking the standard deviations of the one hundred perturbed values of $\delta_s + \delta_c$, and finally, in accordance with 'external consistency', multiplying by ${\chi^2_{\text{pdf}}}^{1/2}$.

3.4 Specific activity of air

For both 511- and 1294-keV activity, the specific activity a of the air (Bq cm^{-3}) sampled from the synchrotron room was calculated from

$$a = 2^{(\delta_c/t_{1/2})}\,\dot{c}\;/\;(\alpha\,\varepsilon\,V_{\mathrm{vessel}})$$

where δ_c is the synchrotron-room-to-HPGe-detector delay time, $t_{1/2}$ is the half-life of the corresponding radionuclide, $\dot{c}$ is the count rate of the 511- or 1294-keV component of the gamma-ray spectrum when the synchrotron is running steadily (*e.g.* the count rate corresponding to the 'high flat' parts of the 15-minute-counts data shown in Fig. 4), α is the emission probability ('abundance') of the gamma-rays being counted, and ε is the full-energy-peak efficiency for counting gamma-rays from the activated air vessel of volume V_{vessel} just in front of the HPGe detector. The full-energy-peak efficiency for the HPGe detector at 511 keV was calculated as $\varepsilon_{511} = 0.0122 \pm 0.0024$ by integrating the point-source full-energy-peak efficiency of the detector over the surface area of the inside of the activated air vessel using MORSE [10] with the DLC37F library [11], and the full-energy-peak efficiency at 1294 keV was integrated in a similar way over the volume of the vessel to give $\varepsilon_{1294} = 0.00388 \pm 0.00078$ (the range in air of the 385-keV-mean-energy positrons from ^{11}C, ~100 cm, is much greater than the characteristic dimension of the vessel, and so most positrons annihilate on the inner surface of the vessel). In view of the conclusion of Sect. 3.1 and anticipating the conclusion of Sect. 3.5 that the 511-keV component is largely due to ^{11}C, from the half-lives of ^{11}C and ^{41}Ar of 20.3 and 110 minutes respectively, and from the gamma-ray emission probabilities per becquerel for ^{11}C and ^{41}Ar of 1.9952 and 0.9916 respectively, results for the specific activity a are presented in Table 2. Representative values for the specific activities of ^{11}C and ^{41}Ar in the air in the synchrotron room are ~0.10 and ~0.03 Bq cm^{-3} respectively.

3.5 Search for ^{13}N component of 511-keV activity

The extent to which the 511-keV activity is due to ^{11}C was investigated by simultaneously fitting the 511- and 1294-keV counts $C_{511,i}$ and $C_{1294,i}$ in the 15-minute bins i during beam-on-to-beam-off transitions with the expressions

$$C'_{511,i} = C'_{^{13}\mathrm{N},i} + C'_{^{11}\mathrm{C},i} + b_{511}(t_i - t_{i-1}) \text{ and}$$

$$C'_{1294,i} = C'_{^{41}\mathrm{Ar},i} + b_{1294}(t_i - t_{i-1})$$

where the $C'_{A_Z,i}$'s are the expressions $C'(t_1,t_2) = \int_{t_1}^{t_2} c'(t)\,dt$ given in the Appendix with $t_1 = t_{i-1}$, $t_2 = t_i$, $\lambda = \lambda_{A_Z} + r_{\mathrm{exch}}/V$ where $\lambda_{A_Z} = \ln(2)/t_{1/2,\,Z_A}$, $t_{1/2,\,Z_A}$ is 9.96, 20.3 and 110 minutes for ^{13}N, ^{11}C and ^{41}Ar respectively, V is the volume of the synchrotron room (25000 m^3) and $w = 4$ minutes. The expressions for $C'(t_1,t_2)$ were used because during the measurement of the time for air to be moved by the ventilation systems from the shutter voids to the synchrotron room (see Sect. 3.3) it was observed that by the time a short burst of smoke in the shutter void had reached the synchrotron room it had spread out in time over ±4 minutes. The seven fitted parameters are $c_{0,^{13}\mathrm{N}}$, $c_{0,^{11}\mathrm{C}}$, $c_{0,^{41}\mathrm{Ar}}$, b_{511}, b_{1294}, r_{exch} and t_{off} where $c_{0,^{13}\mathrm{N}}$, $c_{0,^{11}\mathrm{C}}$ and $c_{0,^{41}\mathrm{Ar}}$, are the steady-state count rates c_0 in the expressions in the Appendix for ^{13}N, ^{11}C and ^{41}Ar respectively, b_{511} and b_{1294} are the corresponding background rates for the 511- and 1294-keV signals, r_{exch} is the air exchange rate at the position where the measurements are being made, and t_{off} is the beam-off time (since beam-off times are not synchronised with the ‘15-minute clock’ of the gamma-ray counting régime). Results are given in Table 3, and one of the fits is shown in Fig. 7. From Table 3, it is clear that the 511-keV activity is nearly all due to ^{11}C, in agreement with the earlier conclusion in Sect. 3.2 — and, incidentally, in accordance with the suggestion [4] that on balance most of the 511-keV air activity is more likely to be due to ^{11}C than to ^{13}N. From the numbers in Table 3, it is evident that the upper limit for the ^{13}N component of the 511-keV activity is at most one tenth of the ^{11}C component.

3.6 Comparison with results from discharge stack monitor

Air from the ISIS synchrotron room is exhausted to atmosphere through a filtered stack (the stack is included schematically in Fig. 1), and a drum-and-Geiger-tubes system [4] is used to monitor the activity in the air being discharged. The sensitivities of the monitoring system are respectively 5330 ± 690 and 3730 ± 340 Bq m^{-3} cps^{-1} for ^{11}C and ^{41}Ar in air, decay-curve measurements show [4] that essentially two-thirds of the activity is due to ^{11}C and one-third to ^{41}Ar, and the system typically counts at rates in the range of 25–30 cps. Consequently, including decay of ^{11}C and ^{41}Ar over the 10 minutes it takes on average for air to be circulated once through the synchrotron room [4], the specific activity of the air in the synchrotron room deduced from the stack monitor is 0.174 ± 0.026 Bq cm^{-3} — a value consistent with the results from the HPGe detector in the present work.

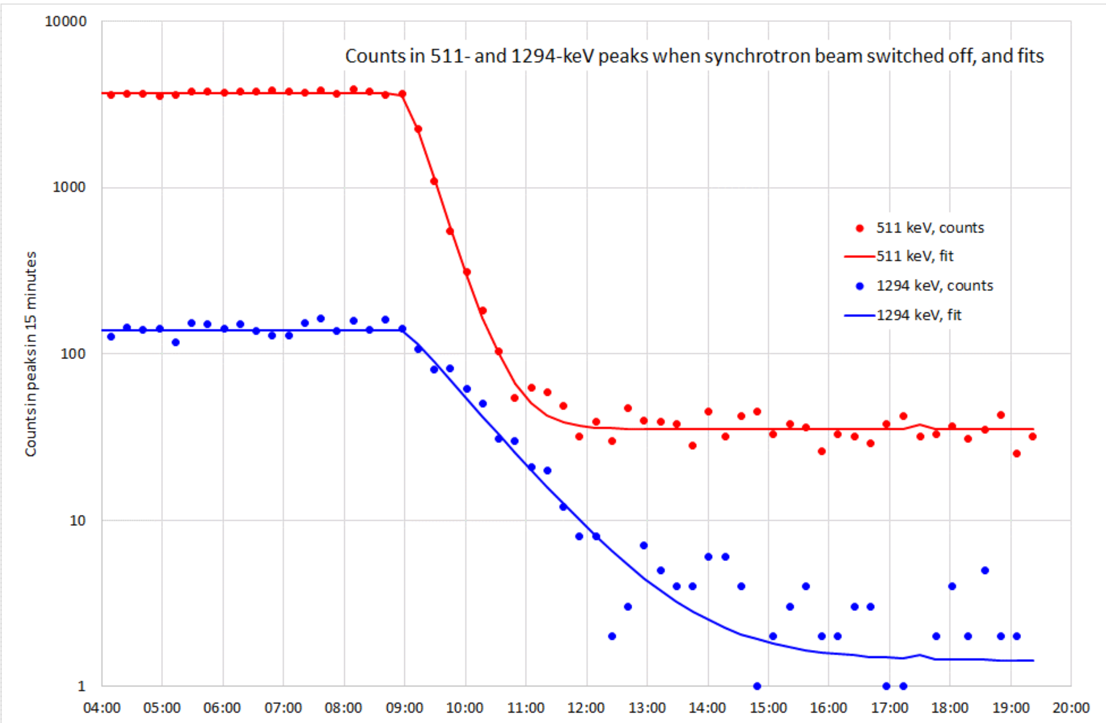

Fig. 7. Typical 7-parameter simultaneous fits to 511- and 1294-keV lines when synchrotron beam is switched off. This fit is for the December 2018 data, where the activated air was sampled close to the inner side of the synchrotron ring between superperiods 5 and 6.

3.7 Comparison of measured and calculated activities

In ref. [3], saturation specific activities of the air in the ISIS synchrotron room were calculated using MCNPX and CINDER-90 [6, 7]. As already mentioned, these were very preliminary calculations with a likely uncertainty of some ±50%, but the result was a total saturation specific activity of 0.56 Bq cm^{-3}, not so very different, given the inevitable approximations and uncertainties involved, from the measured result.

4. Discussion

Why, contrary to the expectation from the Monte Carlo calculations [3] referred to in Sect. 3.2 that ^{13}N should make the largest contribution to 511-keV activity, might the 511-keV activity in the air in the synchrotron room be largely due to ^{11}C? A first possible explanation could simply be that the Monte Carlo calculations did not include all routes for the production of activity. The calculations included incident neutron energies up to 25 MeV, which ought to be sufficiently high to include most of the $^{14}N(n,2n)$ cross-section [12] for the most plentiful component (nitrogen) of air especially in view of the $\sim E^{-3/2}$ energy dependence [13] of the spallation neutron spectrum, but it may be that higher-energy neutrons that induce spallation reactions in the air play a part. Neglecting the difference between neutron-induced and proton-induced spallation, the cross-sections for the production of ^{11}C and ^{13}N from nitrogen and oxygen by spallation lie in the ranges ~10–20 and ~5–10 millibarns respectively [14]. In order to produce a saturation activity of ~0.10–0.15 Bq cm^{-3} (see Table 2) in the air in the synchrotron room by spallation, the effective flux of neutrons inducing spallation in the TS-1 shutter void would have to be $\sim 4–5\times10^{5}$ cm^{-2} s^{-1}, and such a flux is not entirely inconsistent with the geometry and materials in the TS-1 monolith and the TS-1 neutron source term of 2×10^{16} s^{-1} [15].

A second possible explanation could be that some chemical or filtering process preferentially removes ^{13}N from the air (air from the shutter voids does pass through HEPA filters). It could be that the nitrogen activity is accompanied by radiolytic production of NO_X (nitrogen oxide), some of the NO_X being then effectively removed chemically through combination with water vapour [16]. Such a possibility is not inconsistent with corrosion of metal surfaces observed in practice in and around the TS-1 target monolith.

A third possible explanation could be, in principle, that after its production the activated air takes so long to reach the HPGe detector that the ^{13}N has mostly decayed. But it was seen in Sect. 3.3 that the delay time between production of activity and detection of activity in the HPGe gamma-ray detector is ~12–20 minutes, and this is consistent with the delay time of 22 ± 2 minutes [4] observed between production of activity and detection of activity in the drum-and-Geiger-tubes system monitoring the activity of air discharged from the synchrotron room, since it takes several minutes for air from the synchrotron to reach the drum-and-Geiger-tubes monitoring system whereas it takes only ~1 minute for air from the synchrotron to reach the HPGe detector. But even if the overall production-to-detection delay time were as much as 20 minutes, ^{13}N activity would decrease relative to ^{11}C activity by a factor 2, and the application of such a factor to the results of the Monte Carlo calculations would be far from sufficient to reproduce the apparent paucity of ^{13}N in the measured data.

All things considered, the most plausible explanation is that spallation plays an important part in activation of the air and that the chemical removal of ^{13}N is not negligible. It may be noted that in the NuMI facility at Fermilab [17] and in spallation at KEK [18] the measured values of ^{11}C and ^{13}N specific activity in activated air are in the ratios of 1.6 : 1.0 and 2.3 : 1.0 respectively. It would be worthwhile to perform Monte Carlo calculations with highly detailed models of the entire ISIS TS-1 and TS-2 monoliths (including detailed models of the shutters and detailed models of the target, reflector and moderators (TRAM) assemblies) and tracking all particles with energies up to 800 MeV, but the effort to perform such calculations would not be trivial.

It is noticeable in Table 1 that overall source-to-detection times $\delta_s + \delta_c$ are one or two minutes greater for air sampled from near superperiods (SPs) 0 and 9 than for air sampled from near SPs 5 and 6. This is not inconsistent with the facts that these two air-sampling positions (near SPs 0 and 9 and near SPs 5 and 6) are on opposite sides of the synchrotron ring and that activated air from the shutter voids enters the synchrotron room nearer SPs 5 and 6 than SPs 0 and 9.

And it is noticeable in Table 2 that specific activities of both ^{11}C and ^{41}Ar in the air are smaller for air sampled from near SPs 0 and 9 than for air sampled from near SPs 5 and 6, and that ratios of specific activity fall essentially into two sets, the ^{11}C-to-^{41}Ar ratio for air sampled from near SPs 0 and 9 SPs 5 and 6 being smaller than the ^{11}C-to-^{41}Ar ratio for air sampled from near SPs 5 and 6. These differences may be due to the activated air 'spreading out' as it is circulated through the synchrotron room.

5. Summary and conclusions

Measurements of air activation in the synchrotron room of the ISIS Spallation Neutron and Muon Source have been made over a period of time spanning two years. Typical specific activities of ^{11}C and ^{41}Ar in the air in the synchrotron room were found to be ~0.10 and ~0.03 Bq cm^{-3} respectively, but little or no ^{13}N was found. The total specific activity of ~0.13 Bq cm^{-3} is consistent with specific activities found independently using a drum-and-Geiger-tubes system [4] to monitor the air being discharged from the synchrotron room.

There is good evidence that the air in the synchrotron is activated in the shutter voids in the massive shielding monoliths surrounding the neutron-producing targets.

There is plausible evidence that measured specific activities and measured source-to-detector times are consistent with expectations based on the known layout of the synchrotron room.

References

[1] https://www.isis.stfc.ac.uk

[2] J W G Thomason, Nucl. Instr. Meth. A917 (2019) 61.

[3] F Burge and G P Škoro, 'Radiation doses from air activation in the ISIS synchrotron', internal ISIS report, 8 October 2012.

[4] F Burge *et al.*, Nucl. Instr. Meth. A1013 (2021) 165640.

[5] S Karbassi and A Nilsson, ISIS internal report, July 2021.

[6] MCNPX 2.7.0 — Monte Carlo N-Particle Transport Code System for Multi-Particle and High-Energy Applications, https://mcnpx.lanl.gov/

[7] W L Wilson *et al.*, Proc. SARE4 Workshop, Knoxville, USA, 1998.

[8] B Jones, S A Fisher and A Pertica, Proc. 10th Int. Particle Accel. Conf., Melbourne, June 2019, p 2701.

[9] S Karbassi and A Nilsson, ISIS internal report, June 2021.

[10] N P Taylor and J Needham, ‘MORSE-H: A Revised Version of the Monte Carlo Code MORSE’, AERE-R 10432, 1982.

[11] L J Baker and N P Taylor, ‘The Harwell Version of the DLC37F Nuclear Data Library’, AERE-R 11849, 1985.

[12] ‘JANIS Book of neutron-induced cross-sections’, https://www.oecd-nea.org/jcms/pl_44624/janis-books

[13] D J S Findlay, Appl. Radiat. Isot. 121 (2017) 61.

[14] S G Mashnik *et al.*, report LA-UR-97-2905.

[15] D J S Findlay, ISIS internal report, ISIS-DJSF-21-06-B, June 2021.

[16] R P Morco *et al.*, Corrosion Eng., Sci. Technol., 52 (2017) 141.

[17] I L Rakhno *et al.*, Nucl. Inst. Meth. B414 (2018) 4.

[18] A Endo *et al.*, https://www.researchgate.net/publication/237592652_Characterization_of_11C_13N_and_15O_produced_in_Air_through_Nuclear_Spallation_Reactions_by_High_Energy_Protons

Date of measure-ment	Location	Counts / 15 minutes, 511 keV	Counts / 15 minutes, 1294 keV	Bq cm^{-3}, ^{11}C	Bq cm^{-3}, ^{41}Ar	Bq cm^{-3}, ^{11}C ÷ Bq cm^{-3}, ^{41}Ar
Feb. 2018	Foil change area, SP0	1500 ± 50	100 ± 5	0.083 ± 0.017	0.034 ± 0.007	2.5 ± 0.1
Mar. 2018	SP0/9 datum points	550 ± 25	40 ± 5	0.030 ± 0.006	0.014 ± 0.003	2.2 ± 0.3
May 2018	SP9 datum point and SP6 bridge	1550 ± 50	105 ± 10	0.086 ± 0.018	0.036 ± 0.008	2.4 ± 0.2
Jul. 2018	Inner side of SP5/6	4200 ± 200	155 ± 15	0.233 ± 0.049	0.053 ± 0.012	4.4 ± 0.5
Oct. 2018	Inner side of SP5/6	2900 ± 150	100 ± 10	0.161 ± 0.034	0.034 ± 0.008	4.7 ± 0.5
Dec. 2018	Inner side of SP5/6	3700 ± 150	140 ± 15	0.205 ± 0.043	0.047 ± 0.011	4.3 ± 0.5
Apr. 2019	Inner side of SP5/6	4000 ± 200	150 ± 15	0.222 ± 0.047	0.051 ± 0.012	4.4 ± 0.5
Dec. 2019	Inner side of SP5/6	4550 ± 200	155 ± 10	0.252 ± 0.053	0.053 ± 0.011	4.8 ± 0.4
Feb. 2020	Inner side of SP5/6	2000 ± 100	100 ± 10	0.111 ± 0.024	0.034 ± 0.008	3.3 ± 0.4
Means and standard deviations				0.099 ± 0.070	0.032 ± 0.013	
				0.131 ± 0.071		

Table 2. Specific activity of air samples from the synchrotron room when the synchrotron was running steadily. Although there are nine sets of data, there are data sets for only four distinct locations, and so the six measurements made in the same place have themselves been averaged before the means and standard deviations are taken. The uncertainties have been obtained by the same method as that described in the caption to Table 1. In the rightmost column the uncertainties are the statistical uncertainties from the counts in the peaks in the gamma-ray spectrum only, as the detection efficiency of the HPGe gamma-ray detector is a common factor in the ^{11}C and ^{41}Ar specific activities. Whilst in the February 2020 data set the timing data were unavailable, as indicated in Table 1, count rates with the beam on and off were still perfectly visible. Although this table encompasses measurements made over a period of two years, it is perfectly reasonable to form the averages set out in the table because internal ISIS physical configurations and ventilation arrangements for the synchrotron room and target stations (fan speeds, air flow paths, *etc.*) were all always the same during these two years.

Location	Date	$c_{0,^{13}\mathrm{N}}$ min^{-1}	$c_{0,^{11}\mathrm{C}}$ min^{-1}	$c_{0,^{41}\mathrm{Ar}}$ min^{-1}	b_{511} min^{-1}	b_{1294} min^{-1}	r_{exch} m^3 s^{-1}	t_{off} mins.	χ^2_{pdf}
SP0	Feb. 2018	-67 ± 17	163 ± 17	6.4 ± 0.1	2.8 ± 0.1	0.08 ± 0.01	3.8 ± 0.3	± 2.0	1.20
SP0 (no –ve's)		$0\,^{+0.02}_{-0}$	96.0 ± 0.4	6.4 ± 0.1	2.9 ± 0.1	0.08 ± 0.01	3.7 ± 0.4	± 1.0	1.33
SP9, 6	May 2018	-89 ± 27	183 ± 27	6.9 ± 0.1	2.4 ± 0.1	0.08 ± 0.03	3.5 ± 0.5	± 3.8	1.93
SP9, 6 (no –ve's)		$0\,^{+0.15}_{-0}$	93.1 ± 0.5	6.7 ± 0.2	2.4 ± 0.1	0.07 ± 0.03	3.5 ± 0.5	± 1.5	2.12
SP5,6	Dec. 2018	$6\,^{+36}_{-6}$	223 ± 21	8.6 ± 0.1	2.2 ± 0.1	0.09 ± 0.03	4.1 ± 0.4	± 0.9	1.91

Table 3. Results of seven-parameter fits to beam-on-to-beam-off transitions, with inclusion of rectangular time-dispersion function of half-width 4 minutes as described in the text (the February, May and December 2018 data sets are the only data sets for which the timing bins are 15 minutes wide and in which there is at least twelve hours of steady running before beam-off and twelve hours after beam-off to establish background). The uncertainties have been obtained by the same method as that described in the caption to Table 1. The values of the chi-squared of the fit per degree of freedom χ^2_{pdf} are also shown. The three sets of data were each first fitted allowing all seven parameters to have complete freedom; when unphysical negative numbers for the ^{13}N contribution to overall activity were found for the 'SP0' and 'SP9, 6' data sets, these two data sets were re-fitted with very little resultant increase in χ^2_{pdf} whilst constraining all seven parameters to be ≥ 0 thereby showing the ^{13}N contribution to be minimal (these two re-fitted data sets are labelled 'no –ve's')). The absolute value of t_{off} is irrelevant, as all that matters is the uncertainty with which it can be defined. The fitted value of r_{exch}, the rate of air exchange in the synchrotron room, is a little greater than the nominal air extraction rate of 2 m^3 s^{-1}, but this may be a consequence of likely non-uniform patterns of air movements within the synchrotron room.

Appendix

Let the transition at time zero between a constant count rate and a decaying count rate be described by: $c(t) = c_0, t < 0;\ c(t) = c_0 \exp(-\lambda t), t \geq 0$.

Let the count rate $c(t)$ be smeared by the rectangular function:
$s(t') = 0, t' < -w;\ s(t') = 1/(2w), -w \leq t' \leq w;\ s(t') = 0, t' > w$.

If the smeared count rate is $c'(t) = \int_{t-w}^{t+w} c(t')\, s(t - t')\, dt'$, then:
$c'(t) = c_0, t < -w$;

$c'(t) = \{c_0/(2w)\}\{w - t + (1 - \exp(-\lambda(t + w)))/\lambda\}, -w \leq t \leq w$; and

$c'(t) = \{c_0 \exp(-\lambda t)/(2w\lambda)\}\{\exp(\lambda w) - \exp(-\lambda w)\}, t > w$.

The integral of the smeared count rate between times t_1 and t_2 $C'(t) = \int_{t_1}^{t_2} c'(t)\, dt$ is given by summing one or more of the three following integrals with appropriate choices of the limits τ_1 and τ_2 $(\tau_1 \leq \tau_2)$:

$I_1(\tau_1, \tau_2) = c_0(\tau_2 - \tau_1)$, τ_1 and τ_2 both $< -w$;

$I_2(\tau_1, \tau_2) = \{c_0/(2w)\}\{w(\tau_2 - \tau_1) - ({\tau_2}^2 - {\tau_1}^2)/2 + (\tau_2 - \tau_1)/\lambda - (\exp(-\lambda w)/\lambda^2)(\exp(-\lambda\tau_1) - \exp(-\lambda\tau_2))\}$, τ_1 and τ_2 both $\geq -w$ and $\leq w$; and

$I_3(\tau_1, \tau_2) = \{c_0/(2w\lambda^2)\}\{\exp(\lambda w) - \exp(-\lambda w)\}\{\exp(-\lambda\tau_1) - \exp(-\lambda\tau_2)\}$, τ_1 and τ_2 both $> w$.

For example, if $t_1 < -w$ and $t_2 > w$,
$C'(t_1, t_2) = \int_{t_1}^{t_2} c'(t)\, dt = I_1(t_1, -w) + I_2(-w, w) + I_3(w, t_2)$.